Chapter 4

Towards the critical point

4.1 Introduction

The liquid–gas phase transition of small clusters of sodium at atmospheric pressure is discussed in chap. 3. For the bulk matter this first order phase transition has a critical point at a pressure of $p_{c\,\infty} = 253$ atm and a temperature of $T_{c\,\infty} = 2503.7$ K [FL95]. There the density is $\rho_{c\,\infty} = 219\ \mathrm{kg \cdot m^{-3}}$ [FL95] which corresponds to a packing fraction of $\kappa_{c\,\infty} = \frac{v_0}{v_c} \approx 0.3$ (where v_0 is the Wigner-Seitz volume of an atom of sodium, assuming that it is a sphere of radius 2.3 Å and v_c is the critical specific system volume). Hence, one can naturally ask whether systems with a few hundreds of atoms also present a critical point in the sense given in sec. 2.3 on page 30 in chapter 2. I.e. by means of properties of the local curvature of the microcanonical entropy surface. The latter is a function of the energy and of the system volume. If there is a second order phase transition, one can further ask about the physical properties of an ensemble of systems at this transition (pressure, density, mean mass distribution, etc.) and how they can be related to their bulk values (scaling properties).

In this chapter several attempts to reach the critical point of the liquid–gas phase transition of finite size clusters are presented. First, within the cluster MMMC model introduced in the previous chapter with different technics to estimate NCC ($\sim$ the avoided volume to the clusters). Second, as the previous MMMC model approach fails due to computational difficulties (see below), a new model, inspired from lattice gas models, is presented. This new model shows for the time the critical point of the liquid–gas transition of such finite size physical models.

4.2 mmmc results

NCC from EOS

In chapter 3, the caloric curves are obtained from MMMC using the hard spheres equation of states (EOS) approximation to estimate NCC (see app. A.1.2). At atmospheric pressures, there is a first order phase transition. The Maxwell line gives the transition parameters. The specific enthalpies at the two end points of the Maxwell construction are noted by h_1 (liquid side) and h_3 (gas side).The specific latent heat of the transition is defined as $h_3 - h_1$ (see sec. 2.2.3). In the bulk, at the critical point, these two points merge, i.e. the latent heat vanishes.

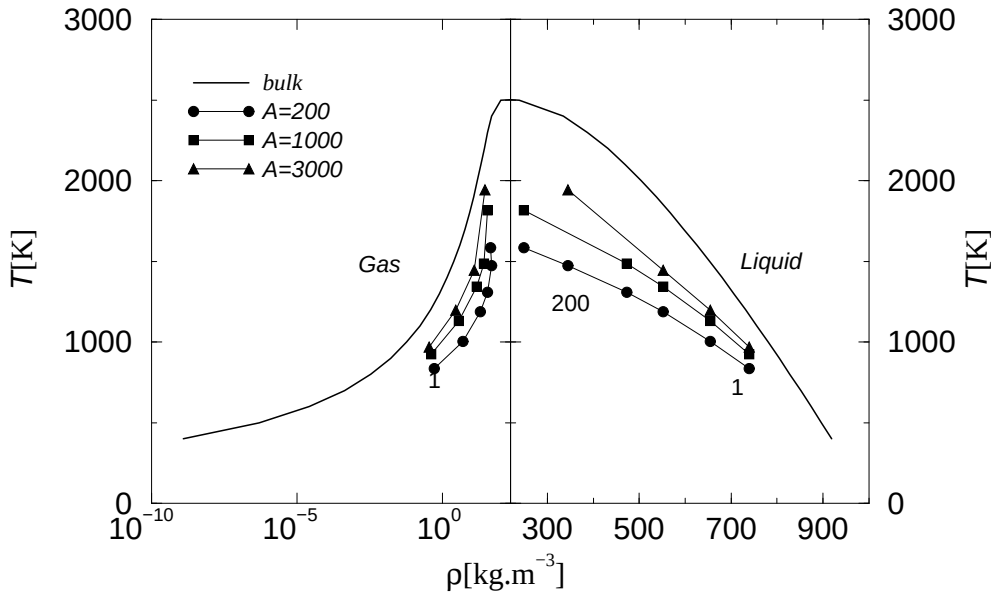

Figure 4.1: Temperature versus density ρ at h_1 (liquid side) and h_3 (gas side) given by the Maxwell construction for different system sizes and pressures ($p = 1$, 10, 50 100, 200, 300 atm, the latter is well above the bulk critical pressure $p_{c\,\infty} = 253$ atm), compared to the bulk liquid and gas densities along the saturation curve (solid line, no symbol) [FL95]. The computations are done within MMMC95 with NCC derived from the hard spheres equation of state (see app. A.1.2). For small pressures there is a clear tendency towards the bulk curves. None of the finite size curves are closed for $p = 300$ atm, this is perhaps an indication that the critical for small systems is located at larger pressures than the bulk one.

As a first attempt to reach the critical point of finite size sodium clusters (if it exists), one can use the same procedure as in the previous chapter and compute caloric curves at constant pressure for higher values of p. Then, one can check whether a critical point shows up, i.e. whether $h_3 - h_1 \to 0$.

In fig. 4.1 the transition temperatures are plotted versus the liquid and the gas density at h_1 (liquid) and h_3 (gas) for different pressures (from 1 atm up to 300 atm) and for several system total masses $A = 200$, 1000 and 3000. The curves shows a clear tendency towards the bulk saturation density curve with increasing A. However there is no critical point, i.e. no curve is closed even for a pressure as large as 300 atm (for $A = 200$ and $A = 1000$). The latter pressure is well above the bulk critical one. One can even see that the gas density for $A = 200$ *decreases* for $p > 200$ atm.

At these high pressures a closer study of the simulation outputs shows that

(a) almost all the pressure comes from the avoided volume pressure term p_{NCC} (up to 80 %),

(b) the system volume V is actually *too small* to contain all the clusters of a typical mass distribution.

The latter point is due to the approximation used to estimate NCC, the avoided volume.

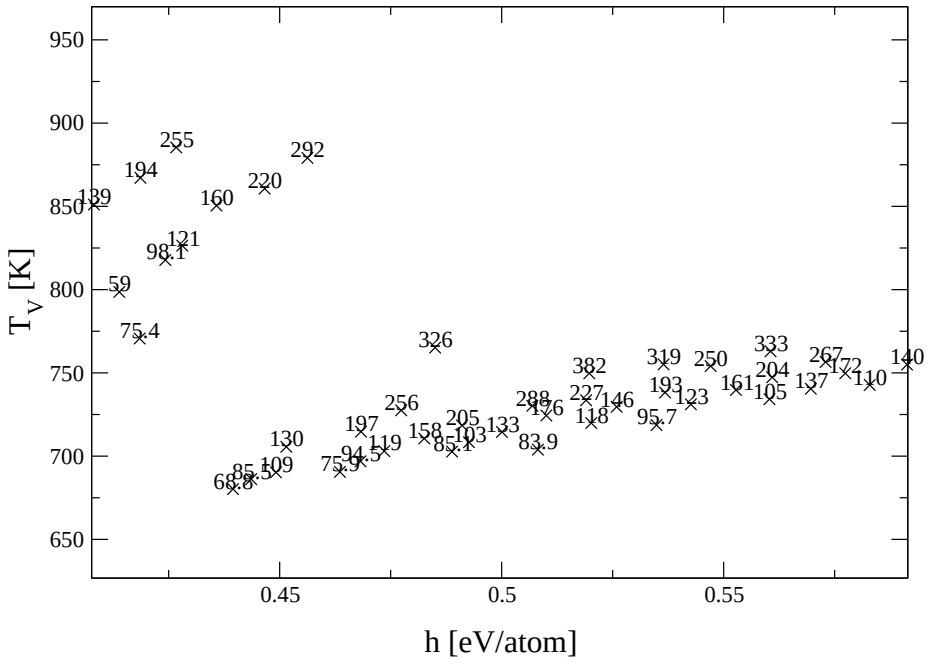

Figure 4.2: Temperature (cross) and pressure (number) as functions of the specific enthalpy h for various values of (E, V) near the multifragmentation transition. The system total mass is $A = 100$. NCC is estimated by means of the Monte–Carlo algorithm presented in app. A.2. Clearly for $p \approx 350$ atm there is still an enthalpy region where $\frac{\partial T^{-1}}{\partial h}|_{p=cst}$ is positive (at $h \approx 0.52$ there is a point $(T_V, p) \approx (750, 382)$ whereas there is at $h \approx 0.46$ a point for which $(T_V, p) \approx (870, 292)$, therefore the isobar $p = 382$ have an higher temperature at $h = 0.47$ than at $h = 0.52$). Hence, the critical point of this model, if it exists, is located at a pressure larger than 350 atm, which is well above the bulk value.

As already mentioned this approximation is based on the hard spheres EOS, which is in its turn based on two body correlations. In this approximation, the critical packing fraction is $\kappa_c = 1$. This packing fraction, where NCC diverges, is unrealistic (for the closest packing of equal size hard spheres $\kappa_c \approx 0.74$). Hence, for pressures larger than one hundred atmospheres, in the transition region, the system is no longer in the range of volumes where higher correlations can be neglected. There, the EOS approximation is not valid and MMMC95 do not sample the correct mass distributions. In other words, by using the EOS approximation some mass distributions have a *finite* NCC although they actually do not fit within the system volume which should imply an *infinite* NCC.

NCC from Monte–Carlo

As there is no other suitable approximations of NCC available for the MMMC model, one has to use Monte–Carlo sampling schemes in order to estimate NCC (see app. A.2).

In fig. 4.2 the temperature along with the pressure as functions of the enthalpy are plotted for several points in the parameter space (E, V) toward the multifragmentation transition. The system total mass is $A = 100$. One can immediately conclude that there is *no critical point* for such model for pressures below 382 atm, i.e. if there is a critical point for this cluster model then it is located at a pressure much larger than the bulk one

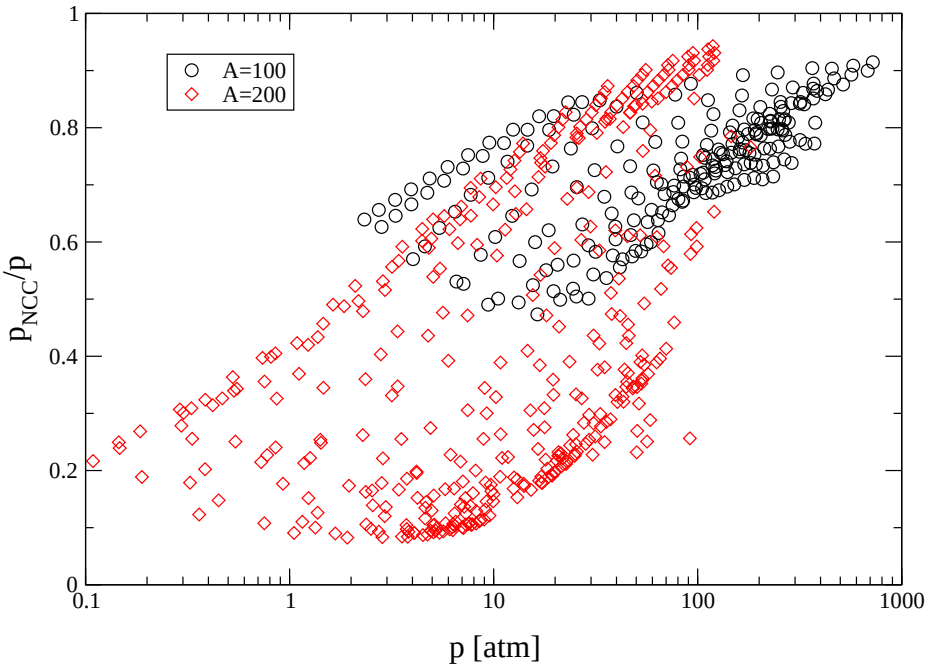

Figure 4.3: Scatter plot of the relative proportion of $p_{NCC} = \beta^{-1}\langle\frac{\partial \ln NCC}{\partial V}\rangle$, the avoided volume pressure (see sec. 3.3), in the total pressure $p = p_{kin} + p_{NCC}$ as a function of p for $A = 100$ (circles) and $A = 200$ (diamonds). Each point in the figure corresponds to one point in the energy–volume plane. As the total pressure increases, the main contribution to p comes from p_{NCC}.

(see figure caption).

For such high pressures, p_{NCC} the avoided volume pressure is the dominant term in the total pressure $p = p_{kin} + p_{NCC}$ for enthalpies below and in the transition region. At higher enthalpy the kinetic term provides again the main contribution. To illustrate that, a scatter plot of p_{NCC}/p versus p is shown in fig. 4.3 for several points in the (E, V) plane near and below the multifragmentation transition. The system total masses are $A = 100$ (circles) and $A = 200$ (diamonds). For pressures larger than 100 atm, p_{NCC} is at least responsible of 60 % of the total pressure in the transition region. This shows how it is crucial to have accurate estimates of NCC and of its derivatives.

These results confirm the ones obtain in the previous section. They suggest that the critical point of finite size clusters is located at higher pressure than the bulk one, e.g. $p_{c\,A=100} > 380$ atm. To check this hypothesis, one should follow isobars at larger pressures. Unfortunatly, this is an impossibly difficult task within MMMC. The typical computation time for one single point in the (E, V) plane for pressures around 150 atm and near the multifragmentation for $A = 200$ is one day on an ALPHA-workstation. This time grows *exponentially* with decreasing volume. More than 99 % of the run time is spend in the numerical estimate of NCC and its derivatives. Thus, a complete study of the transition region at higher pressures is at this moment out of reach.

One may suggest to study smaller systems because less computational efforts should be needed in order to estimate NCC if the number of fragments is reduced. It is indeed the case. However, on the other hand, the critical point seems to be located at even

higher pressures and hence closer to the critical packing fraction where NCC diverges [a]. There, it is very difficult to obtain good estimate of NCC and evenmore of its derivative with respect to the volume (needed to compute p_{NCC}, the main component of the total pressure).

4.3 Lattice model (cl)

At this moment the critical point is out of reach to MMMC95. As written above, this is due to the very long time needed to estimate NCC, which is defined as a multiple integral of the centers of mass of the clusters over the system volume (see eq. (A.1a)). One could argue that a solution is to give up this integration, i.e. leaving the weight ω_{NCC} and position explicitly the centers of mass event by event along the Markovian chain. However, in order to have a correct detailed balance, one has to estimate the a priori probability (see app. B.2) to find a set of positions for the centers of mass so that all clusters fit within the volume. This probability is nothing else but the inverse of NCC.

To overcome this main difficulty, a new model is developped. It is inspired from lattice gas models. This new model is called herafter Clusters on Lattice (CL). In CL the *atoms* are first positioned on a lattice. Hence, the a priori probability to position all the atoms on the grid is the same for all events. The price to pay is that the pressure is no longer an observable as in the cluster MMMC model. The reason is that in CL there is no longer any explicit dependence on the sysem volume in the microcanonical weight (in MMMC this dependence is carried by ω_{NCC} see eqs. (3.19) and (3.23) on page 49).

CL uses the MMMC method. It is a microcanonical model. The total energy, mass and volume $V = \frac{4\pi}{3}R^3$ are conserved.

4.3.1 Model

As CL and the cluster MMMC model are very similar, only the differences between them are stressed in the following section.

Clusters

In MMMC the basic elements are the clusters which are assumed to be spherical hard spheres. In CL the atoms are *first* positioned on a lattice. Two neighboring atoms create a link between them. Linked atoms form together *clusters* (for an illustration see fig. 4.4). Hence, a cluster of a given size can have different shapes characterized by e.g. different principal moment of inertia or total number of links l. For a given mass N a cluster can have up to $l_{\max}$ links ($l_{\max}$ depends on the cluster size).

Once the clusters are created, there are almost treated as in the cluster MMMC model.

The underlying lattice used in the present work is a fcc lattice (face-centered cubic) [AM76]. This lattice does not pretend to simulate the real geometrical properties of sodium clusters [CS00]. It is only a way to get rid of NCC and to add some shape dofs. The distance between two sites is adjusted so that the volume of the lattice primitive cell is equal to the Wigner–Seitz volume of an atom $v_w = \frac{4\pi}{3}r_w^3$. The coordinnate number k of fcc is 12, i.e. one site has 12 closest neighboring sites.

[a] This is confirmed by the results presented in the next section.

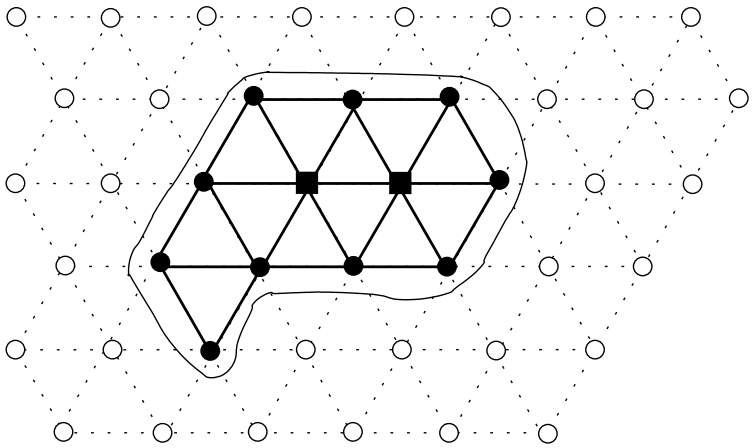

Figure 4.4: Schematic two dimensional illustration of a cluster in CL. An empty lattice site is represented by a circle. A site occupied by an atom is represented either by filled circles or squares. Between two neighboring atoms a link is created (thick segment). An atom whose all neighboring sites are occupied is a volume atom (filled square). In this figure a cluster of size $N = 12$ is represented. It has two volume atoms and 22 links.

In order to have explicit spatial dimensions [b], the center of mass of a cluster is assumed to be located within the volume of a primitive cell $\Delta v = v_w$.

Binding energy

In CL the binding energy of a cluster is a function of N *and* of l, its number of links. This implies a shape dependence of the binding energy.

In the limit $N \to +\infty$ the binding energy is given by

$$E_b(N,l) \approx N\epsilon_\infty \tag{4.1}$$

$$= \frac{2l}{k}\epsilon_\infty, \tag{4.2}$$

where $\epsilon_\infty \equiv -a_v = -1.039$ eV/atom is minus the bulk specific binding energy. In the limit $N \to \infty$, each atom has k neighbors, and there are $l = N\frac{k}{2}$ links. The binding energy of a finite size cluster is given by

$$E_b(N,l) = -\frac{2l}{k}a_v + K(N), \tag{4.3}$$

where $K(N)$ is a constant. For $N > 21$, $K(N)$ is chosen in order to adjust the binding energy of the cluster with the largest number of links (at fixed N) to the metal–drop formula, see eq. (3.1). For $N < 21$, the binding energy of the cluster with the largest number of links (at fixed N) is adjusted to the experimental data. Hence, the electronic shell effects, which are crucial for the presence of the multifragmentation regime (as shown in sec. 3.4.1), are implemented in CL. In the limit $N \to \infty$, $K(N)$ vanishes.

[b] This is needed in order to make the microcanonical weight $\omega(\mathbf{x})d\mathbf{x}$ dimensionless, see sec. 4.3.2.

Internal entropy

For the specific internal entropy $s_{int}(\epsilon^*, N^*, l)$ of a cluster bigger than 3, the same equations as for the cluster MMMC model is used, i.e.

$$N^* s_{int}\left(\epsilon^*, N^*, l\right) \doteq N_s^* s_t\left(\epsilon^*\right) + N_v^* s_\infty\left(\epsilon^*\right), \tag{4.4}$$

where s_t is the trimer entropy given by eq. (3.2) on page 43. s_∞ is the bulk specific entropy obtain from the bulk heat capacity curve (see sec. 3.2 and [GRO97]).

Volume and surface "atoms"

The number of volume atoms N_v^* of a given cluster used in eq. (4.4) to compute its internal entropy is the number of atoms whose all neighboring sites are occupied (squares in fig. 4.4 on the preceding page).

The number of surface "atoms" is simply given by

$$N_s^* = N - 2 - N_v^*. \tag{4.5}$$

In CL a cluster of mass 200 can have up to 76 volume atoms, whereas in MMMC this number is only 56. Hence the specific entropy of the big clusters is larger in CL than in MMMC, whereas for small clusters $N < 12$ the respective internal entropies are the same in both models.

4.3.2 Simulation method

The discussion on the simulation method use for CL is also very similar to the one of MMMC95 (sec. 3.3). The outline of the beginning of this section follows the one of sec. 3.3. To avoid unnecessary repetitions, this section is very brief. For more details the reader should refer to sec. 3.3.

Microcanonical weight

The coordinates of an event are

$$\mathbf{x} \doteq \left\{\mu = \{N_i, l_i\}_{i=1}^{N_f}, \{E_i^*\}\right\}, \tag{4.6}$$

where μ is a short hand for the mass distribution. The i^{th} cluster is characterized by its mass N_i, number of links l_i and internal excitation energy E_i^*. The positions of the atoms on the grid and μ are two equivalent coordinates.

The microcanonical weight $\omega(\mathbf{x})$ is divided in the following way

$$\omega \equiv \omega_{sym}\, \omega_{pl}\, \omega_r\, \omega_{int}\, \omega_{\Delta v}, \tag{4.7}$$

where ω_{sym} is the quantum symmetrization weight factor, see eq. (3.9). ω_{pl} is the result of the integration over the linear and angular momenta, see eq. (3.10). ω_r is the weight due to the angular part of the clusters eigen rotation, see page 47. ω_{int} is the factor due to the internal dofs of the clusters, see eqs. (3.11) and (4.4). $\omega_{\Delta v}$ ensures a dimensionless probability weight

$$\omega_{v_w} = v_w^{N_f}, \tag{4.8}$$

where Δv is equal to the Wigner–Seitz volume of an atom, i.e. $\Delta v \equiv v_w = \frac{4\pi}{3} r_w^3$. Contrary to eq. (3.12a), there is no ω_{NCC} in eq. (4.8).

ω_{pl} and ω_r depend on the clusters shape via the principal moment of inertia of the clusters. Once the clusters are defined, there are considered in ω_{pl} and ω_r as free to move spatially, i.e. the underlying lattice is forgotten.

Observables

The inverse temperature β is an observable as in MMMC95. However, as there is no explicit dependence on the system total volume in CL, see eq. (4.7), therefore, the pressure is not an observable.

Nevertheless, some information about the pressure and its derivatives with respect to the volume [c] and to the energy are needed in order to define phases and phase transitions, see chap. 2. To overcome this difficulty, one can proceed in the following way.

Consider first a caloric curve at fixed volume. β is nothing else but the derivative of the entropy with respect to the energy at fixed volume. Hence one can integrate at fixed volume the β curve and obtain the entropy $S(E,V)$ at fixed volume. This entropy curve is known only up to a constant.

Now, one can proceed in the same way for different system volumes. Each of these entropy curves is known up to an additive constant. One has to find a way to link them in the volume direction.

At very low energy, the system is composed by only one big cluster. Almost all the excitation energy is in the internal dofs of this cluster. Therefore at very low energy the system entropy $S(E,V)$ can be approximatively written as

$$S(E,V) \approx \log\left(\frac{4\pi}{3}(R-r)^3\right) + C(E), \tag{4.9}$$

where $C(E)$ is a function of E. $\frac{4\pi}{3}(R-r)^3$ is the eigen–NCC of the big cluster of radius r within the system volume of radius R (see eq. (A.4) in app. A.1.1). In eq. (4.9) it is implicitly assumed that the big cluster has a spherical shape. This is verified at very low energy, since large clusters with spherical shapes have the lowest binding energy (largest number of internal links).

Hence the difference of entropy $S(E,V_2) - S(E,V_1)$ between two points in the (E,V) plane at low and fixed E is simply

$$S(E,V_2) - S(E,V_1) = 3\log\left(\frac{R_2 - r}{R_1 - r}\right). \tag{4.10}$$

Eq. (4.10) gives the relative shifts between all the entropy curves at constant volume.

Finally, a spline interpolation method is used in order to have a continuous coverage of the energy-volume parameter space.

Algorithm

The basic idea is very simple. From one event $\mathbf{x} = \{\mu, \{E_i^*\}\}$, a new spatial configuration (i.e. new mass distribution μ') is generated by moving randomly one atom. To get

[c] The accessible volume to the atoms is discrete since they are positioned on a grid. The actual system volume is proportional to the number of cells. In the following, a continuous approximation for the system volume is adopted.

the needed information about μ' (masses, number of links, of volume fragments, inertial tensor), the algorithm from Hoshen and Kopelman [HK76] and a straightforward extension [HBM97] is used (see also [BAB98]). This algorithm has been introduced to study the distribution of clusters in percolation systems. Once the new mass distribution is generated, when needed, the excitation energies of the clusters affected by this move are resampled following the algorithm given in app. B.2.2.

Special care has been taken to fulfill the detailed balance condition. The typical number of events used for averaging is 5.10^6. More events (up to 1.10^8) are needed at low energies and large volumes, and also in the multifragmentation region for small volumes. For five millions of event the typical CPU–time is of the order of 5 minutes.

4.3.3 Results

In this section numerical results are shown. They are first compared with MMMC95 results. At large volumes the caloric curves have a region of negative specific heat capacity. It is the signal of a first order phase transition (see sec. 2.2). Finally the critical end point of this phase transition is shown. This is the first time that the critical point of small clusters liquid-gas transition is found.

Comparison with mmmc95

In fig. 4.5 caloric curves at constant system volume as functions of the excitation energy ϵ^* are shown. One of these curves is a result from MMMC95 (circles, T_{95}), the other from CL (squares, $T_{\rm CL}$). The overall qualitative behaviors are similar. For both curves there is a region of negative specific which signals a first order phase transition. However the temperature from CL is almost everywhere larger than the one from MMMC95.

In order to explain these quantitative differences, the information about the corresponding mass distributions as functions of ϵ^* are plotted in fig. 4.6. An important fact is that there is also, in this model, a multifragmentation regime.

From the figure 4.6 one can conclude that the larger temperature in CL is due to its smallest number of fragments compared with MMMC95.

At very low energies ($\epsilon^* \lesssim 0.15$), $T_{\rm CL} < T_{95}$ although there is in both simulation only one big cluster. This can be partially explained by the largest specific entropy energy in CL [d]. There is another reason. In CL, near the ground state the big cluster maximizes its number of internal links in order to gain some excitation energy by loosing binding energy (see eq. (4.3) on page 74). But, as soon as there is enough energy the shape of the big cluster changes in order to maximize N_v^* the number of volume atoms. This is done by adopting a spheroid shape. But this cluster shape has a larger binding energy. All in all, at $\epsilon^* \approx 0.1$ the big liquid cluster has a larger binding energy and a larger internal specific entropy in CL than MMMC95. This implies a smaller overall temperature in CL.

As the energy increases the big clusters have more degrees of freedom in CL. The clusters can have different shapes. These shape dofs delay the evaporation of light fragments. This is the main reason, along with their larger number of volume atoms, why $T_{\rm CL} > T95$. This explain also the delayed multifragmentation in CL. There the big clusters can stand the "weight-competition" at larger energy with a mass distribution composed by several intermediate fragment sizes.

[d] This phenomenom is also to be seen in MMMC95 when there is no entropy surface term, see sec. 3.4.1. and fig. 3.14 on page 60.

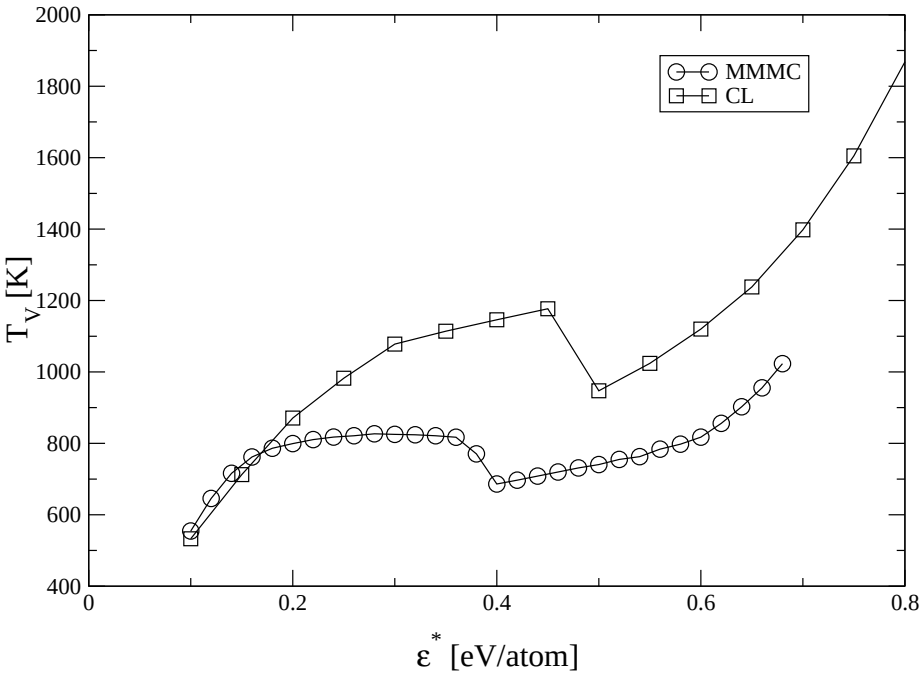

Figure 4.5: Temperatures from MMMC and CL at *constant volume* as functions of the specific excitation energy ϵ^*. For both models the system total mass is $A = 100$ and the system volume is $V \approx 11V_0 = 11\left(\frac{4\pi}{3}Ar_w^3\right)$ where r_w is the Wigner-Seitz radius. The qualitative behaviors of both models are identic. However, the temperature of CL is well above the one of MMMC95 in the transition region. This quantitative differences is related to the differences of the respective mass distributions (see text and fig. 4.6).

Finally, one must stress that CL and MMMC are two models that are qualitatively equivalent but quantitatively different. By tuning the input one can reduce the differences between these models. However, only experimental data (which are at this moment unavailable) can say which model, if any, present the correct behavior.

Critical point

In fig. 4.7 inverse temperature curves as functions of the energy ϵ^* are plotted, each one at constant volume. For systems with a volume smaller than $V_{c'} \approx 3.48\ 10^4$ Å^3 the heat capacity is positive over the whole energy range. Note that $V_{c'}$ does not obligatory correspond to the critical point volume V_c.

At the critical point the following relations hold (see sec. 2.3.1)

$$\lambda_1 = 0, \tag{4.11a}$$

$$\mathbf{v}_1 \cdot \nabla\lambda_1 = 0, \tag{4.11b}$$

where λ_1 is the largest eigenvalue of the Hessian matrix of S and $\mathbf{v}_1$ its associated eigenvector. As discussed in sec. 2.3.2, for a two dimensional parameter system the conditions (4.11) can be simplified to "the lines of constant extensive parameters are tangent to the line $\lambda_1 = 0$".

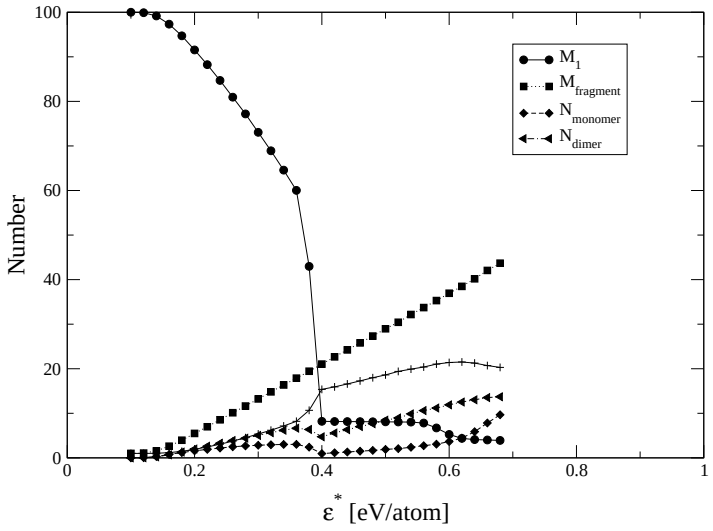

(a) MMMC95

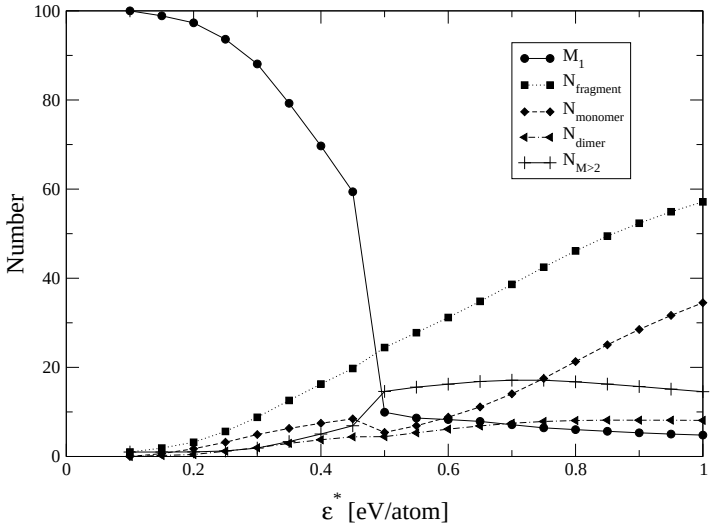

(b) CL

Figure 4.6: Comparisons of mass distributions of CL and MMMC95 at constant system volume as functions of the excitation energy ϵ^*. The system total mass is $A = 100$, its volume V is eleven time the compound cluster volume $V_0 = \frac{4\pi}{3} 100 r_w^3$, where $r_w \approx 2.3$ Å is the Wigner–Seitz radius. M_1, $N_{fragment}$, $N_{monomer}$, N_{dimer} and $N_{M>2}$ are respectively the mean mass of the largest fragment, the mean number of fragments, of monomers, of dimers and of fragments bigger than 2. The qualitative behavior of all the observables are very similar. In particular, in CL there also is a multifragmentation (fast reorganization of the mass distribution) and a multifragmentation regime (evaporation of intermediate cluster sizes).

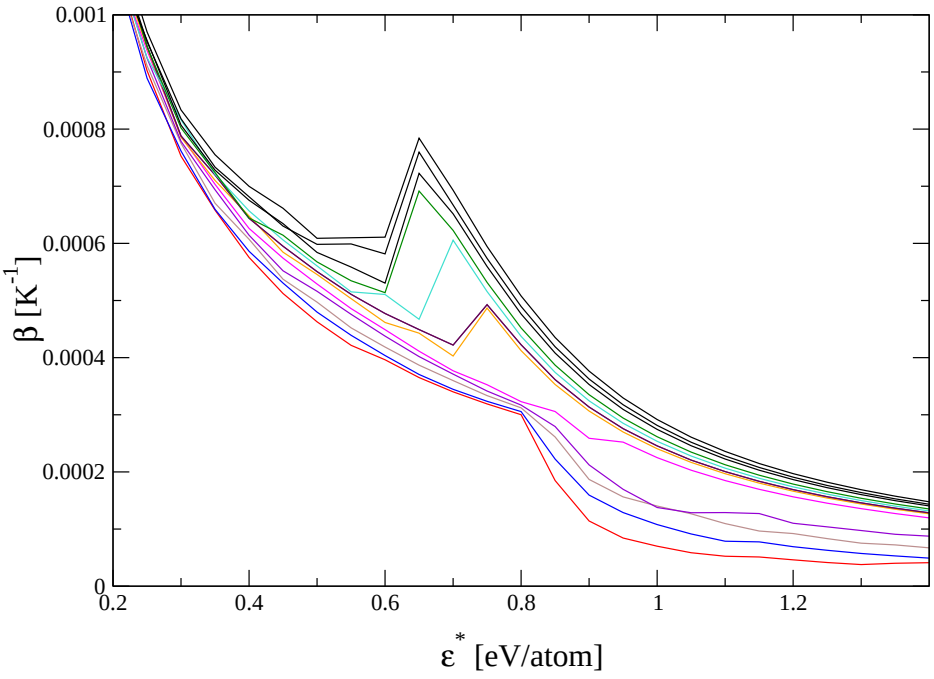

Figure 4.7: Inverse temperature curves at constant volume as functions of the excitation energy ϵ^* and for several system volumes. The system total mass is $A = 200$ and the packing fraction goes from $\kappa = 1.7\ 10^{-4}$ (highest curve) to $\kappa = 0.54$ (lowest curve). For large volume (small κ) a region of negative heat capacity is clearly to be seen. For $\kappa > \kappa_{c'} \approx 0.3$ the back bending vanishes and there is no phase transition in the energy direction. The fluctuations that can be seen at large volumes and at energies below and close to the multifragmentation are not due to statistical errors. They are the consequences of sudden changes of the shape of the big (liquid) cluster. These changes occur when the big cluster looses a "volume" fragment. There it tries to maximize its number of links by adopting a spherical shape. As it looses atoms, it keeps N_v^* fixed by adopting more and more spheroid shape (see text).

From the caloric curves plotted in fig. 4.7 one can infer the entropy and its derivatives in the energy-volume plane as explained in sec. 4.3.2.

In fig. 4.8 the sign of λ_1 along with contour plots of the pressure and the temperature are shown for three system total masses ($A = 100$, 200 and 400) as functions of the specific excitation energy ϵ and of the density given in $\mathrm{kg} \cdot \mathrm{m}^{-3}$.

For all masses, the first order phase transition has a critical end point. This is the first time that critical points are obtained for this type of model. However, their exact locations cannot be deduce from the actual numerical data due to a lack of numerical precision and of the noises generated by the integrations and the spline interpolation used to obtain the entropy surface.

In table 4.1 the critical point parameters, ρ_c, T_c and p_c (the critical density, temperature and mass, resp.) are given for three system sizes $A = 100$, 200 and 300. These parameters are estimated by averaging there respective values within the circles locating the critical points (see figs. 4.8). The errors bars are simply the highest and the lowest values of these parameters within the circles.

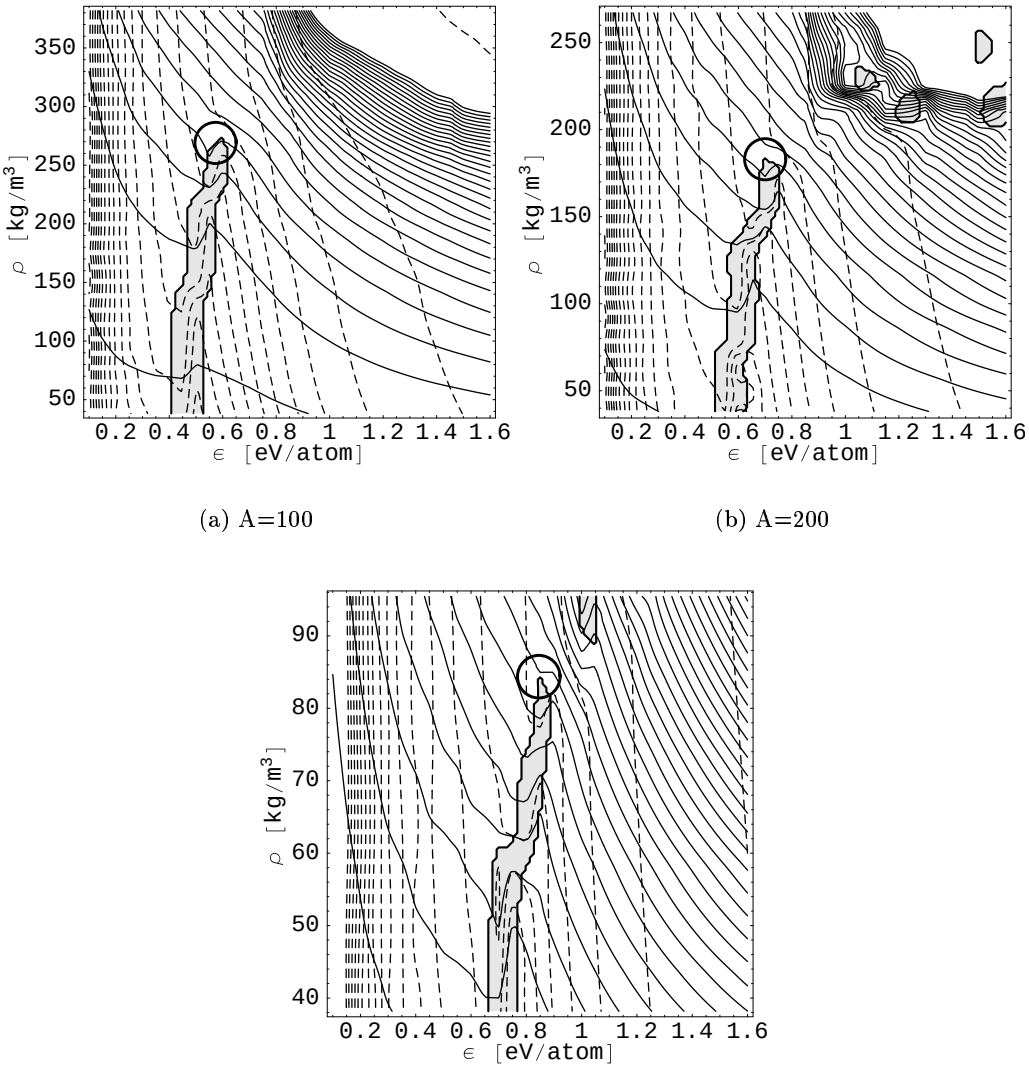

(a) A=100

(b) A=200

(c) A=400

Figure 4.8: Sign of λ_1, the largest eigenvalue of the Hessian of the entropy. λ_1 is positive (negative) in the gray (white) region, $\lambda_1 = 0$ along the thick line. Contour plots of the pressure p and the temperature T, solid and dashed line respectively. All these observables are plotted in the energy-density plane and for several system total masses ($A = 100$, 200 and 400). $\lambda_1 < 0$ implies a pure phase whereas $\lambda_1 > 0$ locates first order phase transition. In the pure phase regions the density at constant pressure and at constant temperature have a "normal" behavior, i.e. $\frac{\partial \rho}{\partial \epsilon}|_{p=cst} < 0$. In the first order transition $\frac{\partial \rho}{\partial \epsilon}|_{p=cst} > 0$. The critical point of this first order phase transition is located where the line of constant pressure (or equivalently of constant temperature) is tangent to the line $\lambda_1 = 0$. The critical points are approximatively located by the thick circles. The regions of positive λ_1 at high density and large energy are due to numerical uncertainties in the caloric curve (see fig. 4.7).

	ρ_c $[\mathrm{kg \cdot m^{-3}}]$	T_c [K]	p_c $[10^3$ atm$]$
100	270 ± 17	2070 ± 200	296 ± 60
200	183 ± 10	2570 ± 170	96 ± 10
400	85 ± 3	2950 ± 230	18.7 ± 2.9
∞	219	2503	0.253

Table 4.1: Critical parameters as functions of the system total mass. ρ_c, T_c and p_c are the critical density, temperature and pressure, respectively. The experimental sodium bulk values are given in the last line [FL95]. The numerical values are estimated from the data shown in fig. 4.8. The errors bars gives the range of values taken by the observables within the circles in fig. 4.8.

Although a simple scaling would not converge to the sodium bulk critical values, they are at least in the correct order of magnitude (apart from the pressure, but one can see that it decreases rapidly with increasing A). These results also confirm the ones from MMMC95 at high pressures. The critical pressure and density *decrease* whereas the critical temperature *increases* with increasing system total mass.

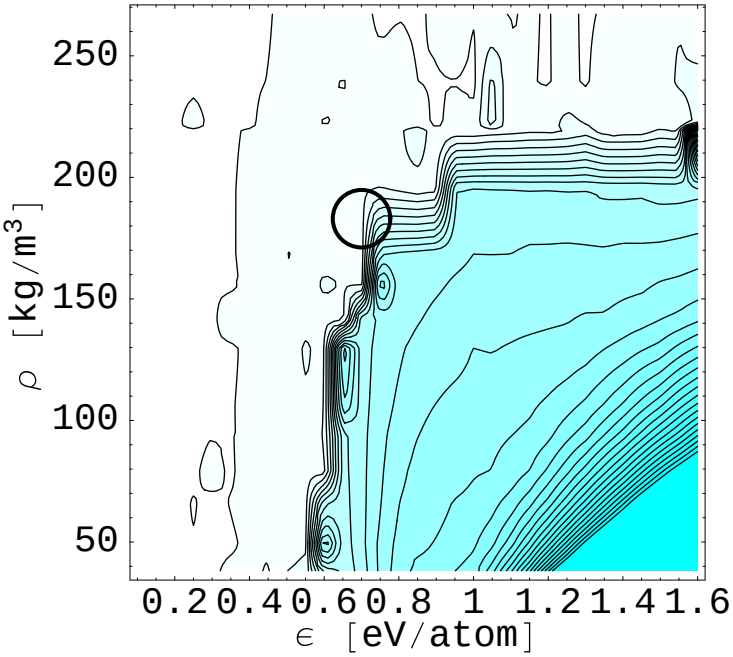

Figure 4.9: Contour-Density plot of the relative fluctuations of $\alpha = \frac{I_{\mathrm{min}}}{I_{\mathrm{max}}}$, the ratio of the smallest principal moment of inertia to the largest one of the biggest cluster in CL toward the critical point in the specific energy-density plane. $A = 200$. The grayer the larger are the fluctuations. The values of σ_α/α is ~ 0.1 at the lower right hand of the figure. The second order phase transition is approximatively located by the circle. Within the available numerical precision α do not exhibit any particular behavior near the critical point. The relative fluctuation increases after the multifragmentation because the principal moment of inertia of small clusters are more sensitive to a shape-changes.

Higher critical density means a more important role of the avoided volume NCC in MMMC95.

The study of this model at high pressures is so far from being complete. Particularly regarding the mass distribution near and at the critical point.

First studies of the mass distribution (and its fluctuations) near and at the critical point do not exhibit any remarkable properties.

As an example, in fig. 4.9 the relative fluctuations of $\alpha = \frac{I_{\min}}{I_{\max}}$, the ratio of the smallest principal moment of inertia to the largest one of the *largest* cluster. This observable probes the shape fluctuations of the biggest cluster. It has been suggested [VOT] that the lack of critical point in MMMC95 is due to the lack of shape dofs in the cluster MMMC model. As one can see in fig. 4.9, nothing special happens near or at the critical point. In particular, the biggest cluster shape does not have large relative fluctuations at the critical point. This result has to be taken with caution. Maybe the absence of large fluctuations are only due to a lack of numerical precision. Further studies, with finer grids are needed.

4.4 Conclusions

In this chapter the liquid-gas transition of small sodium clusters at high pressures is studied.

For small systems the cluster avoided volume (NCC) plays a very important role. In the transition region, its derivative with respect to the system volume gives the main contribution to the total microcanonical pressure. Moreover, the very high values of NCC (see app. A.2) prevent one to study the critical point of the liquid-gas transition of the cluster MMMC model (if it exists at all). These very high values are numerically extremely difficult to evaluate.

A new model inspired from lattice gas models is introduced (CL). By putting the atoms on a fixed grid it avoids the use of NCC. This grids gives new degrees of freedom to the clusters compared to the MMMC cluster model; namely shape-dofs. Moreover, compared to clusters in MMMC, the clusters in CL have a larger number of "volume" atoms for intermediate cluster sizes.

In CL there is no NCC. The price to pay is that the pressure is no longer an observable. The pressure can to be inferred from a set of caloric curves after some integrations and interpolations and by assuming a certain volume dependency of the entropy S at very low energies. All these procedures add a fairly large amount of uncertainty in the numerical evaluation of the derivatives of S with respect to the system volume.

Nevertheless a study of the liquid-gas transition is possible in this model.

At large volumes ($\sim$ low pressures) the caloric curves for CL are very similar to the one of MMMC95. In particular, there is again a multifragmentation. In CL the overall temperature is larger due to (a) a larger number of volume "atoms" implying a larger specific internal entropy at fixed internal energy and cluster size, (b) the new shape degrees of freedom.

As already written, from a set of caloric curves one can infer the entropy surface S in the energy-volume plane. By studying the topological properties of S one can define phases and phase transitions as discussed in chap. 2.

At small volumes (large densities, $\sim$ large pressures), the study of the topology of S shows that the liquid-gas first order phase transition has a critical end point (second order phase transition).

The critical parameters can also be evaluated. Their values are of the order of the bulk ones (except for the critical pressure which is much larger). Qualitatively their values confirm what could be deduced from from the MMMC95 computations. Namely that the critical point is located at lower density and temperature and at higher pressure for finite size systems compared to the bulk critical parameters

However, a simple scaling ansatz shows that these values do not converge to the bulk ones. This is due to all the simplifications made on the physics of the clusters in order to reach this critical point. For example, no highly excited clusters are allowed in CL, although their presence can not be excluded near the critical point (and as shown by preliminary studies). Work is in progress in this direction. As a second example, in CL, the inter-atomic distances are fixed. At very high pressures the atoms can certainly not be simply considered as hard spheres. This effect plays certainly a important role.

Some preliminary results regarding the mass distribution near and at the critical point do not show any particular behavior. Yet, it is unclear if this is simply due to a lack of numerical precision. This will be checked in a near future by performing new simulations with finer grids in the energy-volume plane.